Modelling of Surface Mounted PM Machines Incorporating Saturation Saliency and Frequency Variation

Yi Wang, Jianguo Zhu, Youguang Guo, Yongjian Li, Wei Xu, Jiefeng Hu
School of Electrical, Mechanical and Mechatronic Systems
University of Technology, Sydney
Sydney, Australia
wang.yi@uts.edu.au

Shuhong Wang
Faculty of Electrical Engineering
Xi'an Jiaotong University
Xi'an, China

Abstract—**In this paper a comprehensive magnetic model is developed for a surface mounted permanent magnet synchronous machine (SPMSM) considering both the structural and the saturation saliencies to enable the numerical simulation of new rotor position detection algorithms. With an identifiable parameter matrix, a numerical nonlinear inductance model is proposed, in which the rotor position and the stator current are taken as two independent variables. Additionally, the stator current frequency is taken as another factor of the inductances and the inductances for different frequencies are investigated. After experimentally identifying out all the parameters, a nonlinear mathematic model of SPMSM is built up based on the new magnetic inductance function. Finite element method (FEM) based calculation and simulation results are used to verify the proposed nonlinear magnetic model.**

Keywords- Finite element method; nonlinear magnetic model; permanent magnet synchronous machine; saturation saliency; structural saliency

I. INTRODUCTION

The permanent magnet (PM) electrical machines, e.g. the permanent magnet synchronous machine (PMSM), have found wide applications due to their high-power density (compactness), high efficiency, ease of control, high torque-to-inertia ratio, and high reliability.

The traditional PMSM model is based on the linear magnetic property assumption that the inductance of the stator winding is a constant value for different stator currents. The linear model functions reasonably well in describing the energy conversion and the torque generation inside a PMSM. The widely used field oriented control (FOC) and direct-torque control (DTC) methods were developed based on this linear model and achieved good control performance. A lot of efforts then have been made to improve the PMSM drive performance from the aspects of power electronics, control theory or computing techniques [1]-[3]. However, the application of PMSMs is limited because of the unavoidable rotor-position sensor, which not only increases the system cost, but also perhaps more importantly reduces the system reliability.

A number of techniques for position sensorless and initial rotor position detection have been proposed to reduce the drive system cost and increase the reliability. Most of the schemes are designed based on tracking the rotor magnetic salient pole. However, these sensorless strategies can only achieve good performance for interior PMSM (IPMSM) [4] [5]. They are not suitable for surface mounted PMSM (SPMSM), in which the magnetic saliency is normally very small and hard to detect. On the other hand, the initial rotor polarity could only be detected when the stator core is saturated by adding a large current [6]. The experimental trial and error method has to be employed and it is not possible to numerically simulate the proposed schemes due to the lack of a comprehensive PMSM model incorporating the saturation effect.

The classification of the rotating magnetic saliency inside a PMSM is carried out as the structural saliency that mainly comes from the interior structure, and saturation saliency induced by the magnetic saturation effect of the stator core [7]. Numbers of methods have been proposed to develop a comprehensive PMSM model, among which the finite element method (FEM) based models could achieve accurate calculation for the magnetic field [8]-[10]. However, the FEM based methods require large calculation cost or computing time, even for transient FEM schemes [11]. The developed models could not be applied to machine dynamic simulation.

In this paper, a comprehensive mathematical model of PMSM is built up considering both the structural saliency and the saturation saliency. An SPMSM is chosen as the prototype, in which the saturation saliency is amplified as the main magnetic saliency. A numerical nonlinear inductance model is proposed based on the stator currents and rotor position variation with all the parameters experimentally identified. Furthermore, the inductances at different stator current frequencies should also be considered because a number of sensorless drive strategies are proposed based on high frequency signal injection schemes. In this paper, the stator current frequency is considered as another factor of the values of the stator winding inductances, which are essential for rotor saliency tracking. The FEM based calculation and simulation results are used to verify the machine model. The

comprehensive nonlinear machine model is built up in SIMULINK and this model can be further used to develop, simulate and evaluate the rotor position detection strategies.

II. NONLINEAR MODEL OF PMSM WITH SALIENCIES

In a rotating PMSM, the observable total flux linkage λ_t inside the air-gap is contributed by both the stator currents and the permanent magnets on the rotor. Based on the assumption that the flux in the air-gap is sinusoidally distributed, the three-phase flux linkages λ_{abc} are here defined as the projection of λ_t on the stator reference frame and not only induced from the stator current directly. The voltage equation of the stator windings can be written as

$$v_{abc} = R_s i_{abc} + \frac{d}{dt}\lambda_{abc} \tag{1}$$

where v_{abc}, i_{abc} and R_s are the phase voltages, currents and winding resistance in the stator reference frame, respectively.

The relationship between the current and flux linkage is usually described by the nonlinear magnetization curve. For conventional linear PMSM models, this magnetization curve is always assumed to be linear, and the linear PMSM model is often expressed as

$$v_{abc} = R_s i_{abc} + L_{abc}\frac{d}{dt} i_{abc} \tag{2}$$

where L_{abc} is the three-phase inductance matrix including the self- and mutual-inductances and it is independent of the stator currents.

Therefore, in the rotor reference frame, the *d*- and *q*-axis inductances are thereby constant. When a set of unequal *d*- and *q*-inductances is employed, the structural saliency of a PM machine can be calculated based on this model. However, this linear model could not be used to describe the nonlinear saturation saliency.

For a nonlinear model, the magnetic saturation is considered and the inductances are expressed as incremental inductances variable with the stator current. Then a composite function can be used to express the flux linkage

$$\lambda_a = f(i_{abc}, \theta) \tag{3}$$

where θ is the rotor electrical angle.

Substituting (3) into (1), the following differential equations can be obtained

$$\begin{bmatrix} v_a \\ v_b \\ v_c \end{bmatrix} = R_s \begin{bmatrix} i_a \\ i_b \\ i_c \end{bmatrix} + L^*_{abc}\frac{d}{dt}\begin{bmatrix} i_a \\ i_b \\ i_c \end{bmatrix} + \frac{\partial}{\partial\theta}\begin{bmatrix} \lambda_a \\ \lambda_b \\ \lambda_c \end{bmatrix}\omega_e \tag{4}$$

where $\frac{\partial}{\partial\theta}\begin{bmatrix} \lambda_a \\ \lambda_b \\ \lambda_c \end{bmatrix}\omega_e$ is the rotating back-emf in three-phase windings; L^*_{abc} is the nonlinear inductance matrix which is also a composite function of the stator currents and the rotor position.

III. NONLINEAR INDUCTANCE MODEL

The inductance matrix is the main difference between the conversional linear model and the proposed nonlinear model. A composite function is designed to express the nonlinear inductance matrix.

A. Nonlinear Mathematical Model

As shown above, the variables of stator inductance are the stator currents and the rotor position, which are linear independent [12]. Once the rotor position is fixed, the flux linkage could be expressed in terms of stator current as the magnetization curve.

$$\lambda(i) = k_0^* + k_0 i + k_1 i^2 + \cdots + k_m i^{m+1} \tag{5}$$

where $k_0, k_1, \ldots k_{m+1}$ are identifiable parameters.

The inductance at that rotor position is then defined as

$$L(i) = \frac{d}{dt}\lambda(i) = k_0 + k_1 i + k_2 i^2 + \cdots + k_m i^m \tag{6}$$

The multinomial order, *m* depends on the magnetization curve.

On the other hand, when the stator current magnitude is fixed, the self- and mutual-inductances of the stator windings are periodical function of the rotor electrical position. For the nonlinear machine model, this function will be a non-sinusoidal curve, because of the saturation effect. When the rotor N pole aligns with the stator excitation phase, the inductance value will be smaller than that under S pole. Therefore, this function has to be expressed by using Fourier Serise:

$$L(\theta) = a_0 + \sum_{n=1}^{\infty}\left[a_n \cos(n\theta) + b_n \sin(n\theta)\right] \tag{7}$$

where a_0, a_n and b_n are the Fourier Series coefficients;

n is the Fourier Series order.

Then a composite function of both the current and rotor position is defined to express the inductance

$$L(i,\theta) = I(i)\cdot A \cdot C(\theta) \tag{8}$$

where $I(i) = [1 \quad i^1 \quad i^2 \quad \cdots \quad i^m]$;

$$C(\theta)=[1 \quad \sin(\theta) \quad \cos(\theta) \quad \cdots \quad \sin(n\theta) \quad \cos(n\theta)]^T$$

;

$$A=\begin{bmatrix} a_{0,0} & a_{0,1} & \cdots & a_{0,2n} \\ a_{1,0} & a_{1,1} & \cdots & a_{1,2n} \\ \vdots & \vdots & \ddots & \vdots \\ a_{m,0} & a_{m,1} & \cdots & a_{m,2n} \end{bmatrix}$$ is the identifiable parameter matrix.

In this function, the nonlinear inductance can be calculated and updated against both the current value and the rotor position angle. The function can be applied to both three-phase self- and mutual-inductance curves by varying the parameter matrix *A*. The magnetization curve and Fourier Series orders will be defined later and the parameter matrix will be identified by experimental method.

B. Parameters Identification

An experiment platform is carried out on an SPMSM to identify the parameters and test the inductances. The block diagram is shown in Fig. 1. In order to accurately identify the two-dimensional parameter matrixes, both the rotor position and stator current should be controlled to satisfy the whole variation range. On one hand, the rotor position variation could be controlled mechanically by using the dividing head attached on the rotor shaft. On the other hand, electrical excitation has to be applied to the stator windings to emulate the stator flux and to calculate the incremental inductance values around the operation point on the magnetization curve.

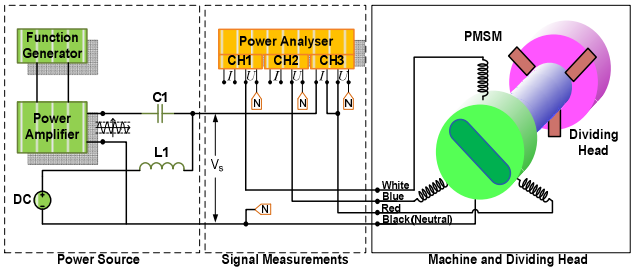

Figure 1. Experiment platform for inductance test.

In this test, a DC offset current vector is applied to the stator windings to simulate an instantaneous condition of the rotating stator current vector, which has a constant magnitude while steady state operation. The amplitude of the offset current determines the saturation effect and will set the operation point to different levels on the magnetization curve.

The inductance at the operation point is defined as the derivative of the flux linkage, which is difficult to measure in the test. An incremental inductance is then defined to represent that value. Based on the DC offset current, an AC excitation signal has to be added to measure the incremental inductance value as shown in Fig. 1.

During the test, the stator currents are fixed at several different levels from 0 to 6A at which the magnetic circuit is fully saturated. For each current offset, by applying a small AC current component the incremental inductance at a particular rotor position is measured. The incremental inductance calculation is shown in Fig. 2.

By changing the rotor position with a dividing head, a series of inductance is recorded with a resolution of 6 electrical degrees. The nameplate parameters of the tested SPMSM are shown in Table I.

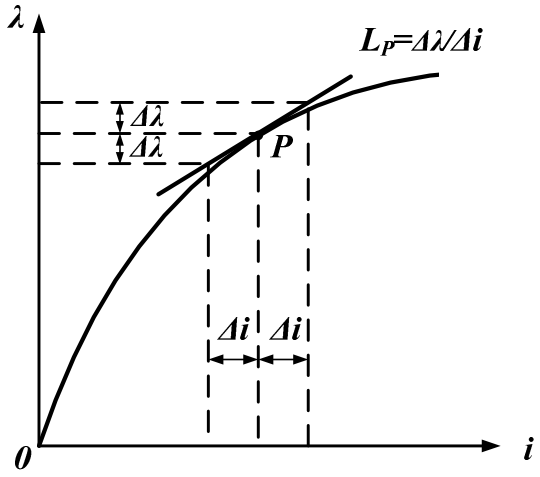

Figure 2. Incremental inductance calculation.

TABLE I. PARAMETERS OF TESTED SPMSM

Name-plate Parameters	Values
Model	IFT 6071-6AC21-2-Z
Number of Poles	6
Rated Power	1000 W
Rated Voltage	128 V
Rated Current	6.5 A
Rated Speed	2000 rev/min
Rated Torque	4.8 Nm

The magnetization curve is usually expressed by using a fifth or seventh order multinomial. In order to fit a seventh order saturation curve, m is set to 6 in (5) and (7).

On the other hand, for the periodical inductance variation on rotor position change, the order of Fourier component vector *C(θ)* is chosen based on the harmonics weights. Fig. 3 shows the inductance curves at different current offset levels. It is found that the harmonics of the inductance mainly converge in the first 8 orders based on the FFT of the inductances at different currents. In order to regress the inductance-position curve accurately, n is set to 8 in (7).

Therefore, the dimension of matrix A is set to 7×17, by setting m=6 and n=8 to acquire an accurate enough surface regression. The composite inductance function can be rewritten as

$$L(i,\theta)=[1 \quad i^1 \quad i^2 \quad \cdots \quad i^m]\cdot\begin{bmatrix} a_{0,0} & a_{0,1} & \cdots & a_{0,16} \\ a_{1,0} & a_{1,1} & \cdots & a_{1,16} \\ \vdots & \vdots & \ddots & \vdots \\ a_{6,0} & a_{6,1} & \cdots & a_{6,16} \end{bmatrix}\cdot\begin{bmatrix} 1 \\ \sin(\theta) \\ \cos(\theta) \\ \vdots \\ \sin(8\theta) \\ \cos(8\theta) \end{bmatrix} \qquad (9)$$

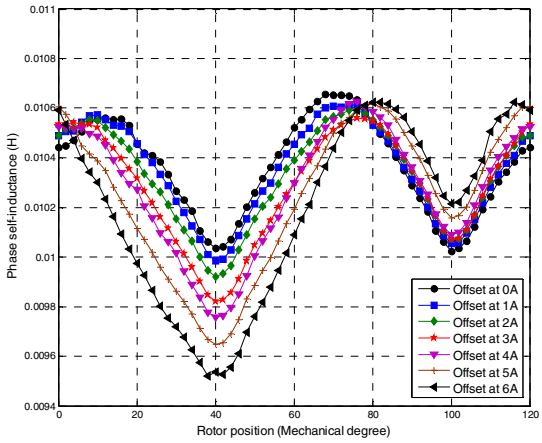

Figure 3. Measured self-inductance curves at different current offset levels.

On the other hand, the inductance variations are small and periodically fluctuant function. To obtain better regression results, the Least Relative Residual Sum of Square (LRRSS) method is employed. For the objective function *L(i, θ)*, the relative residual sum of square is defined as

$$f_{re}(A)=\sum_{i=0}^{6}\sum_{\theta=0}^{2\pi}\left[\frac{I(i)\cdot A\cdot C(\theta)-L_{test}(i,\theta)}{L_{test}(i,\theta)}\right]^2 \qquad (10)$$

The parameter matrix A then could be calculated by using the equations set as

$$\begin{bmatrix} \frac{\partial f_{re}(A)}{a_{0,0}} & \frac{\partial f_{re}(A)}{a_{0,1}} & \cdots & \frac{\partial f_{re}(A)}{a_{0,16}} \\ \frac{\partial f_{re}(A)}{a_{1,0}} & \frac{\partial f_{re}(A)}{a_{1,1}} & \cdots & \frac{\partial f_{re}(A)}{a_{1,16}} \\ \vdots & \vdots & \ddots & \vdots \\ \frac{\partial f_{re}(A)}{a_{6,0}} & \frac{\partial f_{re}(A)}{a_{6,1}} & \cdots & \frac{\partial f_{re}(A)}{a_{6,16}} \end{bmatrix}=0 \qquad (11)$$

A Matlab m-file function is designed to calculate the matrix A based on (10) and (11). Fig. 4 shows the regression result for the self-inductance function. To get a better display, the transpose of A is shown. The relative residual sum of square of this regression, $f_{re}(A)$ is only to 0.1207656%.

Fig. 5 shows the comparison between the tested and estimated self-inductance of phase A at 0A and 6A current offsets, where ±0.5% error bands are added. It can be found that the relative errors of the inductances are very small and the regressed objective function can be used to describe the variable self-inductance.

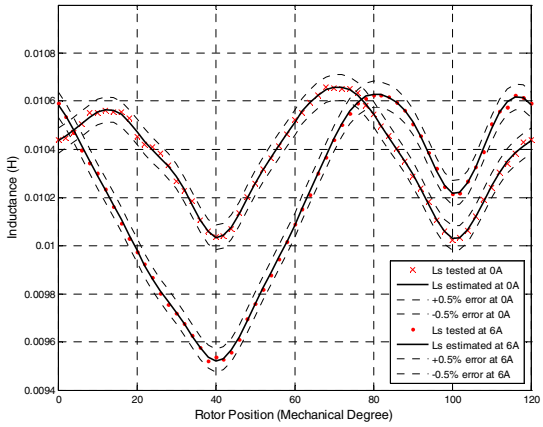

Figure 5. Measured and estimated incremental self-inductance at different current offsets

```
The inductance function is:

L(i,theta)=I*A*C

where I=[1, i, i^2.....i^6]

where C=[1; sin(theta); cos(theta)......sin(8*theta); cos(8*theta)]

Transpose of the identified matrix A are shown below:

 1.033161e-002    1.826616e-004   -2.964326e-004    1.848164e-004   -5.692404e-005    8.441806e-006   -4.792239e-007
 7.961604e-005   -2.178127e-004    2.822324e-004   -1.687079e-004    4.971831e-005   -6.990749e-006    3.751450e-007
-2.697391e-006    5.747257e-005   -1.689034e-004    1.008563e-004   -2.821520e-005    3.692633e-006   -1.848052e-007
-3.245813e-008    3.777973e-006   -3.708625e-006    2.897571e-006   -1.098561e-006    2.013165e-007   -1.345508e-008
-2.151661e-004   -2.982116e-004    4.637074e-004   -2.905583e-004    8.612218e-005   -1.209168e-005    6.483820e-007
-2.023202e-005    3.463247e-005   -4.474151e-005    3.271982e-005   -1.165886e-005    1.892861e-006   -1.131193e-007
 1.384118e-006   -2.343029e-005    4.591333e-005   -2.223562e-005    4.683547e-006   -4.066563e-007    9.739848e-009
 2.220408e-005   -9.910784e-005    1.587962e-004   -1.062460e-004    3.355900e-005   -4.970170e-006    2.778212e-007
-3.835927e-005    1.557006e-005   -2.588199e-005    1.331768e-005   -3.030075e-006    3.012171e-007   -1.025621e-008
-4.111030e-007   -5.058673e-006    1.870218e-005   -1.633403e-005    5.787541e-006   -9.005050e-007    5.132110e-008
 1.838878e-005   -7.676781e-005    1.103879e-004   -6.785370e-005    1.999289e-005   -2.800970e-006    1.501270e-007
-1.955725e-005    8.798353e-005   -1.311051e-004    8.266168e-005   -2.496681e-005    3.572919e-006   -1.945733e-007
-3.544146e-005    6.229436e-005   -8.630772e-005    5.233725e-005   -1.550063e-005    2.208250e-006   -1.208284e-007
 1.263231e-005   -4.902457e-005    6.771658e-005   -4.047151e-005    1.177823e-005   -1.649215e-006    8.885831e-008
-9.385055e-006    3.329189e-005   -4.246642e-005    2.429400e-005   -6.777156e-006    9.033522e-007   -4.610219e-008
 1.094569e-005   -4.734164e-005    6.747005e-005   -4.267503e-005    1.294548e-005   -1.846851e-006    9.960156e-008
 3.200770e-006   -4.736682e-005    6.744323e-005   -4.145098e-005    1.236332e-005   -1.765373e-006    9.658453e-008
```

Figure 4. Curve fitting for self-inductance parameters by using LRRSS method

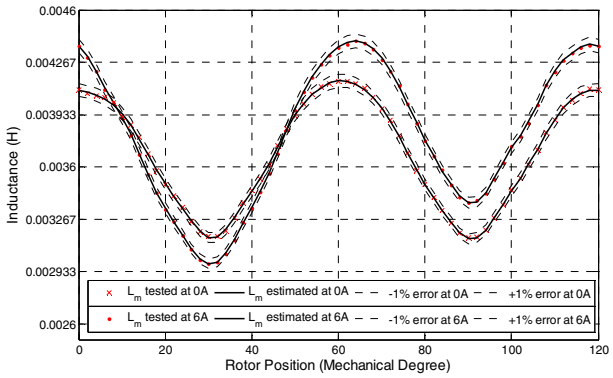

Figure 6. Measured and estimated incremental mutual-inductance at different current offsets

The same regression method is applied to the mutual-inductance coefficients identification. Fig. 6 shows the comparison between the tested and regressed mutual-inductance between phases A and B at different current offsets.

Then a nonlinear inductance model is built up for this three-phase machine. An accurate inductance matrix can be calculated for given stator currents and rotor position. This model incorporates both the machine structural and the saturation saliencies.

IV. Model Verification by FEM

To verify the new nonlinear inductance model, the 2-dimensional FEM is applied to numerically calculate the magnetic field of the machine. The data of the machine physical parameters is collected, including the material characteristics of the magnets and the core. After dismantling the machine, the inner dimensions are also measured. Fig. 7 shows the magnetic field distribution and Fig. 8 shows the comparison of estimated and calculated inductances.

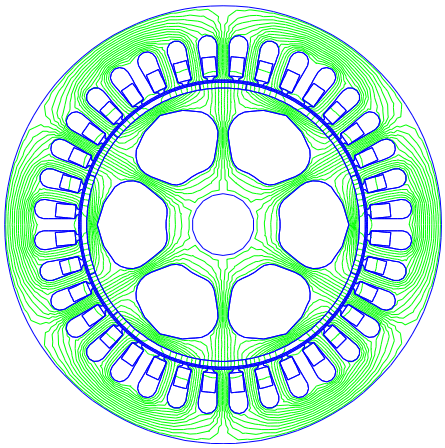

Figure 7. Magnetic field distribution the inductance is calculated.

It can be found that the calculated inductances approximately coincide with the estimated values. The errors shown in Fig. 8 mainly come from the stator skewed slots. The ending leakage inductances of the stator windings and the skewed slots on the stator are not considered in this 2-dimensional FEA algorithm. The stator leakage inductance is calculated separately and the value is about 1.9mH.

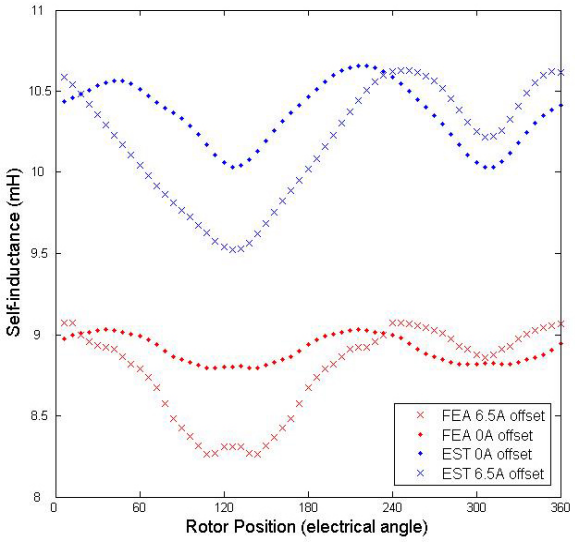

Figure 8. Comparison of the estimated and calculated self-inductances.

V. Inductance Variation versus Frequency

As shown above, the inductance of the SPMSM is related to the stator current amplitude and the magnet rotor position. On the other hand, the inductance values are also varying against the stator current frequency, which is always varying in the machine drive system. In most of the proposed initial rotor position detection schemes, the injection signal frequency is set at a much higher value in order to keep the rotor at standstill and to amplify the inductance variation.

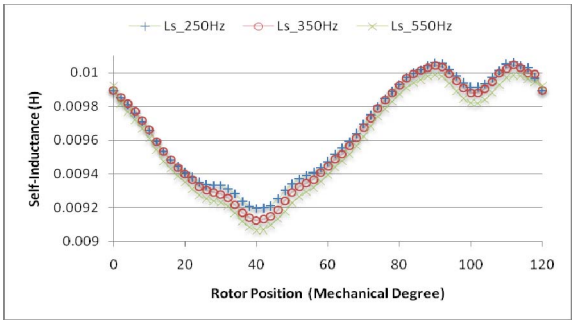

Figure 9. Measured self-inductance curves at different current frequencies.

On the same experiment platform, the inductance tests are carried out on different frequencies. Fig. 9 shows the inductance curve at different current frequencies, which are chosen at high frequency levels. The current offset level is set at 6A and the rotor angle varies.

It can be found that the self-inductance values vary with the current frequency, but the profiles of the curves are close, which indicates that the saturation saliency is almost constant for different frequencies. For different frequency operation, the rotor magnetic saliency has the same traceable position. Once

an injection scheme is proposed, the injected signal frequency will only affect the practical impedance values but not the profiles of the impedance curves.

VI. MACHINE PERFORMANCE

A comprehensive nonlinear three-phase inductances model is built up in SIMULINK, based on which the mathematical model of the SPMSM is built in MATLAB/SIMULINK as well. This new model is different from the linear machine model given in the SIMULINK library. Both the structural saliency and the saturation saliency are accounted in the new model.

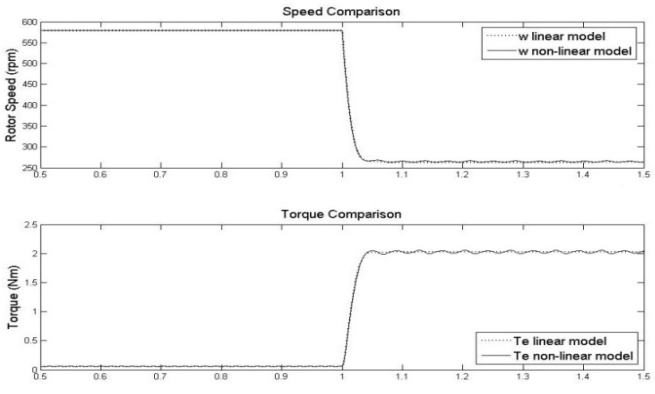

Figure 10. Comparison of speed and torque at no-load and load change.

The new machine model is then simulated with open loop drive method. It is started without load and then a load torque is mounted on the rotor shaft, at which the three-phase stator inductances are saturated. The machine speed and torque output curves are plotted in Fig. 10.

It can be found that when the machine runs at no-load the output torque is stable because the three-phase inductances are unsaturated and the equivalent d- and q-axis inductances are almost constant which induce a constant torque output on the shaft.

On the other hand, after the load torque is stepped up, the stator currents rise and the stator core is saturated. There are ripples on the speed and torque output caused by the saturated and asymmetry inductances. These features make the simulation more accurate, which do not exist in the linear machine model simulations.

VII. CONCLUSIONS

In this paper, a nonlinear model of PMSM is developed based on a composite inductance function, which is designed to express the inductance as the function of both the stator current and the rotor position which are de-coupled.

An experimental platform is carried out to identify the inductance coefficients. After taking a set of inductance measurements, the self- and mutual-inductances at different current levels and different rotor positions are recorded. The LRRSS method is employed to identify parameters and the regression results are verified by FEM calculation. According to the FEM results, the nonlinear inductance model is reasonable and effective to simulate the real machine. The stator current frequency is investigated as another variable of the inductance matrix. The self-inductance curves are plotted at different stator current frequencies. The modelled result shows that the profile of the inductance curves is the same. The variation of the inductance values is small and does not make any change of the rotor magnetic saliency position.

With the identified coefficients, the new SPMSM model is built up in MATLAB/SIMULINK. The effect of the saturation saliency can be found from the simulation results. Based on this new comprehensive model, simulation of the proposed novel drive methods will be possible which will avoid the experimental trial and error process, reduce the development cycle time and save the research costs.

REFERENCES

[1] P. Pillay and R. Krishnan, "Control characteristics and speed controller design for a high performance permanent magnet synchronous motor drive," *IEEE Trans. Power Electron.*, vol. 5, no. 2, pp. 151-159, 1990.

[2] C. Lascu and A. M. Trzynadlowski, "Combining the principles of sliding mode, direct torque control, and space-vector modulation in a high-performance sensorless AC drive," *IEEE Trans. Ind. Appl.*, vol. 40, no. 1, pp. 170-177, Jan./Feb. 2004.

[3] L. A. Cabrera, M. E. Elbuluk and D. S. Zinger, "Learning techniques to train neural networks as a state selector for inverter-fed induction machines using direct torque control," *IEEE Trans. Power Electron.*, vol. 12, no. 5, pp. 788-799, Sept. 1997.

[4] M. E. Haque, L. Zhong and M. F. Rahman, "A sensorless initial rotor position estimation scheme for a direct torque controlled interior permanent magnet synchronous motor drive," *IEEE Transactions on Power Electronics*, Vol. 18, No. 6, pp.1376–1383, Nov.2003.

[5] L. Tang, L. Zhong, M. F. Rahman and Y. Hu, "A novel direct torque control for interior permanent magnet synchronous machine drive system with low ripple in torque and flux-a speed sensorless approach**",** *in Proceedings of IEEE Industry Applications Society Annual Meeting*, Oct. 2002, Vol. 1, pp.104–111.

[6] Y. Jeong, R. D. Lorenz, T. M. Jahns, and S. K. Sul, "Initial rotor position estimation of an interior permanent-magnet synchronous machine using carrier-frequency injection methods," *IEEE Transactions on Industrial Applications*, Vol. 41, No. 1, pp. 38–45, Jan./Feb. 2005.

[7] Y. Yan, J. G. Zhu, Y. Guo and H. Lu, "Modeling and simulation of direct torque controlled PMSM drive system incorporating structural and saturation saliencies," *in Proceedings of the 41st IEEE Industry Application Society Annual Meeting*, Tampa, FL, Oct 2006, pp. 76-83.

[8] O. A. Mohammed, S. Liu, and Z. Liu, "Physical modeling of pm synchronous motors for integrated coupling with machine drives," *IEEE Trans. Magn.*, vol. 41, no. 5, pp. 1628-1631, May 2005.

[9] Dong-Myung Lee, and Woo-Cheol Lee, "Analysis of relationship between abnormal current and position detection error in sensorless controller for interior permanent-magnet brushless dc motors," *IEEE Trans. Magn.*, vol. 44, no. 8, pp. 2074-2081, Aug. 2008.

[10] P. Sergeant, F. De Belie, and J. Melkebeek, "Effect of rotor geometry and magnetic saturation in sensorless control of pm synchronous machines," *IEEE Trans. Magn.*, vol. 45, no. 3, pp. 1756-1759, Mar. 2009.

[11] W. N. Fu, S. L. Ho, and Z. Zheng, "Design of position detection strategy of sensorless permanent magnet motors at standstill using transient finite-element analysis," *IEEE Trans. Magn.*, vol. 45, no. 10, pp. 4668-4671, Oct. 2009.

[12] P. Cui, J. G. Zhu, Q. P. Ha, G. P. Hunter, and V. S. Ramsden, "Simulation of non-linear switched reluctance motor drive with PSIM," *in Proceedings of the 5th International Conference on Electrical Machines and Systems*, Vol. 1, Aug. 2001, pp. 1061-1064.